The Monte Carlo Method: Versatility Unbounded In A Dynamic Computing World
Chattanooga, Tennessee, April 17–21, 2005, on CD-ROM, American Nuclear Society, LaGrange Park, IL (2005)

GEANT4 SIMULATION OF AN OCULAR PROTON BEAM AND BENCHMARK AGAINST OTHER MONTE CARLO CODES

David R Shipley and Hugo Palmans
Quality of Life Division
National Physical Laboratory
Teddington, United Kingdom
david.shipley@npl.co.uk; hugo.palmans@npl.co.uk

Colin Baker
School of Health Sciences
University of Liverpool
Liverpool, United Kingdom
colin.baker@liverpool.ac.uk

Andrzej Kacperek
Douglas Cyclotron
Clatterbridge Centre for Oncology
Bebington, Wirral, United Kingdom
andrzej.kacperek@ccotrust.nhs.uk

ABSTRACT

This paper describes recent work using GEANT4 to simulate monoenergetic proton beams (50 MeV, 150 MeV and 250 MeV) and the 62 MeV ocular proton beam line at the Clatterbridge Centre for Oncology (CCO). GEANT4 results are compared with those obtained using other Monte Carlo codes (MCNPX, PTRAN, and SRIM) and measurement, including depth-dose data and radial dose and energy distributions at two different depths.

GEANT4 and PTRAN are in generally good agreement but differences in both the depth and height of the Bragg peak become more apparent at higher energies due to the parameterisation in GEANT4 of stopping power data taken from ICRU 49, and by some differences in their inelastic nuclear interaction cross-section data. Other variations at the energies under consideration are accounted for by PTRAN's lack of secondary proton transport. GEANT4 is in better agreement with MCNPX at all energies but again differences in the nuclear interaction data result in MCNPX giving a higher relative dose compared to GEANT4 at depths below the Bragg peak. The different multiple scattering model used in MCNPX also tends to give broader radial dose distributions and significantly larger tails in the energy distributions in water compared to GEANT4.

Further simulations of depth dose and radial dose distributions in PMMA are compared with diode and film measurements on the CCO ocular proton beam line. GEANT4 overestimates the height of the Bragg peak for the full-energy beam by around 20% and gives a slightly increasing (instead of a flat) dose profile for the modulated beam with a distinctive peak near the end of the range. Radial dose profiles are in reasonable agreement with measurement although GEANT4 produces a sharper penumbra. However, daily variations in the beam output and the type of detector have a significant effect on the measured data.

Key Words: proton, dosimetry, geant4

1 INTRODUCTION

The Douglas Cyclotron within the Clatterbridge Centre for Oncology (CCO) is the only proton therapy facility in the United Kingdom, and has an energy suitable for treating various forms of eye cancer. There are presently over a dozen centres in the world offering this type of treatment. One of the attractive characteristics of a proton beam is the narrow Bragg peak, which can be spread out uniformly over a certain depth using range modulation. This results in the tumour receiving a homogeneous dose, with negligible dose beyond the proton range.

Many accurate Monte Carlo methods and techniques have been developed for use in conventional radiotherapy involving X-rays, γ-rays, and electrons [1, 2]. This is not, however, the case in proton therapy where the physics of proton dosimetry remains relatively unexplored. Current treatments are predominantly based on calculations using one-dimensional pencil beam algorithms that are assumed to be sufficiently accurate for most purposes [3]. However, the presence of strong inhomogeneities, such as within the head and neck regions, tend to have a significant effect on the accuracy of these simulations and therefore the treatments that are based on them. More complex pencil-beam algorithms [4] and a Monte Carlo based treatment planning system for proton beams [5] are currently in development.

In this paper, the GEANT4 Monte Carlo code [6] will be used to resolve some of these dosimetry issues in low-energy proton beams. Depth dose characteristics (peak to entrance ratio, Bragg peak width) and radial dose characteristics (rms lateral deflection for pencil beams) as well as distributions of proton energy are calculated using GEANT4 for a number of mono-energetic proton beam energies. All these will then be compared with calculations performed in other work with the following three Monte Carlo codes: PTRAN [7], a system of codes for calculating the transport of protons with initial energies between 50 and 250 MeV in homogeneous water, MCNPX (version 2.5d [beta release]) [8, 9], a general purpose N-particle code similar to GEANT4, and SRIM (version 2003.12) [10], a group of programs for determining the stopping power and range of ions in matter.

The more difficult challenge of simulating range-modulated and full-energy beams from the CCO proton therapy facility, that is similar to most other low-energy clinical proton beam lines, is also described. In particular, depth-dose and radial-dose distributions for these beams calculated using GEANT4, MCNPX and McPTRAN.RZ are compared with diode and film measurement. McPTRAN.RZ is a derivative of PTRAN developed by Palmans [10] for simulating proton beams in a cylindrical-slab geometry. In all cases, the possible reasons for any observed discrepancies between the different codes and the measurements will be discussed.

2 METHOD OF CALCULATION

2.1 Description of the Codes

A new GEANT4 code WaterPhantom was developed to calculate the depth-dose and radial-dose distributions for a series of proton beams incident on the front face of a phantom. Depth-dose was obtained by scoring the total energy deposited in a series of 200 cylindrical slabs of varying thickness and radius centred on the beam axis, and, radial-dose was obtained from the total energy deposited in a series of 100 annular rings of varying width placed at a given depth in the phantom. WaterPhantom also scores, and stores in an external data file, the phase space data

(that is, the energy, the position coordinates and the direction cosines) of all particles striking a scoring plane placed at a specified depth in the water phantom. The required energy and angular distributions at a given depth in the phantom were obtained by analysing the raw phase space data using a MATLAB script.

The 62 MeV proton beam line at the CCO described in detail by Bonnett [12] was modelled using a modified version of HadronTherapy, a code supplied as one of the advanced examples with the GEANT4 distribution. All components of the beam line except for the range shifter have been included in the model. In particular, the PMMA modulator wheel that consists of four spokes each with 32 individual slabs was defined precisely giving eight modulator wedges. This can be rotated between 0 and 45 degrees in arbitrary steps using a dedicated messenger class in GEANT4. A final collimator diameter of 30 mm giving a circular beam in the phantom was used in these calculations.

The calculations described in this paper were carried out using GEANT4 release 6.2 (with patch02), the CLHEP version 1.8.1.0 libraries and with the Low Energy Electromagnetic Physics package G4EMLOW version 2.3. The code was installed and compiled on a linux based server and calculations performed on a number of linux computer nodes.

2.2 Physics processes and transport parameters

The Low Energy Electromagnetic Physics package [13] extends the validity of electromagnetic interactions in GEANT4 for a variety of particles to the lower energies that are of particular interest in this work. In particular, the package offers a number of alternative parameterisations to model proton energy loss due to electromagnetic interactions at these energies. In this work, the *ICRU_R49p* parameterisation that is based on ICRU Report 49 [14] was used throughout. However, the 'chemical effect' [15] that becomes significant for ionisation losses of low energy protons below a few MeV, and also implemented in GEANT4, was not used here as it was found to have no significant effect on the calculated depth dose distributions in water at 50 MeV.

GEANT4 also offers a number of hadronic shower models for simulating hadronic interactions in matter. The low-energy and high-energy parameterised driven models (LHEP and HEP) were used in this work to model all hadronic processes relating to elastic and inelastic interactions with the nucleus. Both the low energy electromagnetic physics package and the LHEP and HEP models are generally recommended for use in medical applications of GEANT4.

A cut value of 0.02 mm was used in the phantom region (using the cut per region feature) and a cut value of 10 mm in all other regions. The former cut value is at least an order of magnitude smaller than the smallest region present in the phantom geometry to ensure that energy deposition is determined as accurately as possible and that any dependencies of the particle transport on the geometry are minimized.

2.3 Calculations

Depth-dose calculations were carried out using WaterPhantom for 50, 150 and 250 MeV monoenergetic pencil beams using slab widths of 0.2, 1.0 and 2.0 mm respectively. Energy, angular and radial dose distributions were determined in 10, 30 and 60 mm radius regions for the

same energies at depths of $0.5 \times r_0$ and $0.9 \times r_0$ in the phantom, where r_0 is the proton CSDA range for the given energy.

Simulations of the CCO beam line were performed using a monoenergetic pencil beam of protons with an incident energy of 62.5 MeV (which gives a beam energy of approximately 60 MeV at the front face of the phantom). Depth-dose distributions were scored in a PMMA phantom for both a full-energy (that is, no modulator wheel) and a modulated beam using a slab width of 0.2 mm and a circular beam with a diameter of 30 mm (defined by the final collimator). Radial dose distributions were also determined in 20mm radius regions at the front face and at various depths in the phantom.

3 RESULTS AND DISCUSSION

The depth dose curves in water for 50, 150 and 250 MeV monoenergetic pencil proton beams calculated in this work using GEANT4 are compared with similar curves obtained using PTRAN, MCNPX and SRIM in Figures 1-3. Depth-ionisation data (instead of depth dose) has been plotted for SRIM normalized to the PTRAN entrance dose value. The correction required to convert from ionisation to dose in water is assumed to be small and has not been applied here.

At 50 MeV, it can be seen that there is good agreement between GEANT4 and PTRAN in both the peak-to-entrance dose ratio (PEDR) and the depth of the Bragg peak. However, there is clearly a range difference between these two codes and SRIM, which has a similar PEDR but produces a Bragg peak at a smaller depth. With MCNPX, the range of the protons is similar to GEANT4 and PTRAN but the PEDR is around 15% smaller. In all cases, the width of the Bragg peak (at 50% of the peak dose) is similar for all codes.

The variation in the range of the protons is primarily due to different proton stopping power data being used in the simulations. Both MCNPX and PTRAN use Janni's shell corrections [16] to stopping powers for protons given in ICRU 49 [14]. GEANT4 uses a parameterised stopping power model also based on ICRU 49 (and, by default, derives the mean excitation energy of the material using Bragg's rule), whereas SRIM uses a stopping power model based on the formulism by Zeigler [17].

The proton energy loss straggling model used in the codes affects both the width and height of the Bragg peak. Both PTRAN and MCNPX use the Vavilov energy straggling distribution [18] whereas GEANT4 uses three different straggling models to simulate energy loss fluctuations [19] including one based on the Vavilov distribution. Nuclear interactions of the primary protons lead to a reduction in the number of protons at depth, and so also in the absorbed dose. This reduces the height of the Bragg peak, but at 50 MeV, only around 5% of the proton energy is lost by this process and the effect is small. However, the Bragg peak on the MCNPX curve is around 20% smaller than the GEANT4 and PTRAN indicating differences in the implementation of the energy straggling model or the use of a different multiple scattering model. The SRIM curve is a few percent higher than the other curves at all depths up to the Bragg peak. This is consistent with the fact that SRIM does not model proton energy loss by nuclear interactions and so instead this energy loss contributes to the calculated ionisation.

At 150 MeV, shown in Figure 2, the agreement between GEANT4 and PTRAN depth dose curves is not as close as at 50 MeV. In particular, the Bragg peak obtained with both GEANT4 and MCNPX now occurs at a slightly smaller depth compared to PTRAN. The PEDR for

GEANT4 and MCNPX is now 10 % and 18% smaller respectively than PTRAN. Even though all these codes use similar stopping power models, the implementation and evaluation of these models is different. For example, GEANT4 uses a parameterised fit to the model whereas PTRAN uses lookup tables for proton energy loss based directly on ICRU 49.

Energy losses due to nuclear interactions are much more significant at 150 MeV and 250 MeV (contributing about 20% and 40% of the total energy loss respectively). Consequently, the SRIM curve is now up to 20% higher than the other curves at 150 MeV for the reasons outlined above and so the SRIM results obtained for 250 MeV are not presented. Energy losses at all depths up to the beginning of the Bragg peak are very similar for the other codes at 150 MeV indicating that both the models and nuclear interaction cross-sections used are very similar.

At 250 MeV, shown in Figure 3, the difference in the stopping power data evaluation in the PTRAN compared to GEANT4 and MCNPX has an even more pronounced effect on the depth of the Bragg peak. The discrepancies in the non-elastic nuclear cross sections used in all these codes, indicated by the variation in the height of the Bragg peak and differences in the energy losses at smaller depths, is also more apparent at this energy.

Figures 4 and 5 show the radial dose distributions at depths of $0.5\times r_0$ and $0.9\times r_0$ in water for the three proton energies calculated with PTRAN, GEANT4 and MCNPX, where the CSDA range r_0 has been taken from ICRU 49.There seems to be generally good agreement between PTRAN and GEANT4 over small radii at both depths indicating that these codes use similar multiple scattering distributions. However, the tails of the distributions obtained with GEANT4 extend to much greater radii when compared to PTRAN. This is primarily because PTRAN does not transport secondary protons, unlike MCNPX and GEANT4. The radial dose distributions obtained for MCNPX at both depths are generally broader compared to GEANT4 and PTRAN indicating differences in the multiple scattering models being used in this code. However, the tails of these distributions are similar to GEANT4 at all incident energies indicating that the models are more closely matched for lower energy protons. By default, PTRAN uses the Molière formalism [20] to model multiple scattering of charged particles whereas MCNPX uses a model based on Goudsmit and Saunderson [21]. GEANT4 uses a more complete model for multiple scattering based on the theory of Lewis [22]

Figures 6 and 7 show the energy distributions at depths of $0.5\times r_0$ and $0.9\times r_0$ in water. Variations in the peak energy from one code to another at $0.9\times r_0$ are consistent with the variations in the depth of the Bragg peak noted above. The use of a finite sized slab instead of a plane to score particles in GEANT4 is the most likely reason why the peak at 50 MeV occurs at a smaller energy than the other two codes at 50 MeV, as the position of the peak will be very sensitive to the size of the slab used near the Bragg peak. At $0.5\times r_0$, the energy distributions obtained with the three codes are in good agreement around the peak energy. The low energy tail in the energy spectra at both depths represent the contribution from secondary protons with MCNPX generally producing a slightly larger tail at lower energies than GEANT4: the data from PTRAN have no such tail, since secondary protons are not transported by this code.

The depth dose curves calculated with GEANT4 in a PMMA phantom for both the full-energy and modulated CCO beam with an initial proton beam energy of 62.5 MeV are compared with recent diode measurements [23] in Figures 9 and 10 respectively. Measurements were made in PMMA but no stopping power correction has been applied to this data: each was normalised to the entrance dose. Depth dose curves calculated in PMMA with McPTRAN.RZ and MCNPX are

also shown. The initial proton energy of 62.5 MeV was obtained by finely tuning the MCNPX simulation so that the average energy at the exit of the final collimator was 60 MeV.

For the full-energy beam, again it can be seen in Figure 9 that the GEANT4 and McPTRAN.RZ curves in PMMA are very similar, as expected from the earlier observations in a 50 MeV monoenergetic pencil beam, but overestimate the height of the Bragg peak by 20% when compared with measurement. The MCNPX curve, however, is in better agreement with both sets of measurements matching both the depth and the height of the Bragg peak more closely. The widths of the Bragg peaks are similar in all cases. One should note, however, that the CCO beam output can vary significantly. For example, it can clearly be seen in Figure 9 that variations in both the depth and height of the Bragg peak occur for similar diode measurements performed on different days. The type of detector employed for the measurement of dose distributions can also give different results. Silicon diodes tend to give higher response (typically 7% around the Bragg peak) compared to similar measurements with a parallel plate ionisation chamber [24].

For the modulated beam shown in Figure 10, GEANT4 and McPTRAN.RZ both give a larger relative dose with depth in the phantom compared with measurement and, in particular, produce more distinctive peaks in the dose profile near the end of the range. MCNPX produces a generally flatter dose profile over all depths but with a slightly lower relative dose towards the end of the range. In all cases, the dose profiles near the end of the range are particularly sensitive to the construction around the openings between the fins of the modulator wheel. Only minor adjustments to size of the gap and wheel thickness near these openings was found to have a significant effect on the dose profile. The observed discrepancies in the codes could therefore be partially due to minor differences in the geometry and techniques used to simulate the modulator wheel but they are more likely due to the differences in the physical models used in the codes described previously.

Figures 11 and 12 show the radial dose distributions calculated with GEANT4 for the modulated CCO beam at the front face and at $0.5 \times r_0$ in a PMMA phantom respectively, and compared with both with diode and film measurements (normalised to give the best fit to the calculated data). As mentioned earlier, variations in the measurements tend to be quite large and so the data shown here are obtained from the mean of at least four independent sets of diode measurements and by combining several film profiles both along different axes and from each side of the central beam axis. At the front face, GEANT4 generally gives good agreement with measurement over most of the radial profile up to around 1.2cm. However, there is a distinctive peak towards the edge of the profile compared with measurement. This aspect of the profile near the penumbra is particularly sensitive to the configuration of the final aperture in the beam line that defines the beam size. Although not shown in the measurement data presented here, other measured dose profiles have indicated the presence of these distinctive peaks particularly when close to the final collimator.

The penumbra obtained with GEANT4 is also much sharper than measurement, as shown by the steeper curve at the edge of the profile in Figure 11, but the overall width of the profile is very similar to the film measurement. The diode measurements give a slightly wider profile than film measurement but this may be entirely due to the 1 mm resolution of these measurements with only two measurement points being made in the penumbra region. One should also note than the simulation does not include the cross-hairs that are used to align the beam. This is also likely to have a small effect on the front face profile particularly near the centre of the beam.

The radial profile obtained at $0.5 \times r_0$ with GEANT4 and shown in Figure 12 is also in generally good agreement with film measurement but with GEANT4 again giving a sharper penumbra. In this case, there is no distinctive peak at the edge of the profile, as seen at the front face, confirming that the peak is primarily due to low energy proton scatter from the final aperture.

4 CONCLUSIONS

The work described in this paper has highlighted a number of differences in proton beam simulations with GEANT4, when used with physics list and transport parameters described earlier, and other similar Monte Carlo codes (PTRAN, MCNPX, SRIM). GEANT4 generally agrees with PTRAN in depth dose calculations in water at lower energies (below 150 MeV) but tends to underestimate both the depth and height of the Bragg peak at higher energies primarily due to the method used for deriving the required proton stopping power data and differences in the non-elastic nuclear interaction cross sections. These two codes also agree in their calculation of radial dose and energy distributions around the peak of the distribution with significant differences only occurring at depths towards the end of the range. Unlike GEANT4, PTRAN does not transport secondary protons and so underestimates the tails of these distributions.

GEANT4 is in closer agreement with MCNPX at all energies compared to PTRAN but tends to overestimate the height of the Bragg peak at lower energies. However, the different nuclear interaction cross-sections being used in MCNPX tend to overestimate the dose from these processes at higher energies at depths below the Bragg peak Similarly, MCNPX gives a broader radial dose distribution than GEANT4 at all energies indicating differences in the multiple scattering models used in these codes. The tails of these distributions are however in closer agreement. The energy distributions of GEANT4 and MCNPX are in generally good agreement at these energies but with MCNPX producing a significantly larger tail at lower energies than GEANT4.

When used to simulate a typical ocular proton beam line, such as the one at the CCO, the depth dose curves calculated with GEANT4 in PMMA for both a full-energy and modulated beam have characteristics that closely match those of measured curves. However, GEANT4 overestimates the height of the Bragg peak for the full-energy beam by around 20% and, tends to give a slightly increasing dose profile (instead of a flat profile) for the modulated beam with a distinctive peak near the end of the range. These observed features are very sensitive to the configuration of the modular wheel, particularly around the gaps and, thus may be partially due to minor differences in the geometry and techniques used to simulate the modulator wheel. However, it is more likely that the different physical models used in the codes account for these differences.

The radial dose profiles obtained with GEANT4 for the modulated beam are also in generally good agreement with measurement. However, GEANT4 produces a sharper penumbra than indicated by measurement and the edge of radial dose profile near the surface of the phantom is sensitive to the configuration of the hole in the final collimator. One should note that all measurements are subject to daily variations in the beam output and have some dependence on the type of detector used.

5 REFERENCES

1. I. Kawrakow, "VMC++, electron and photon Monte Carlo calculations optimized for Radiation Treatment Planning ", *Advanced Monte Carlo for Radiation Physics, Particle Transport Simulation and Applications: Proceedings of the Monte Carlo 2000 Conference,* Lisbon, 23-26 October 2000, pp 229 – 236 (2001).
2. D.W.O. Rogers, B.A. Faddegon, G.X. Ding, C.-M. Ma, J. Wei and T.R. Mackie, "BEAM: A Monte Carlo code to simulate radiotherapy treatment units," *Med. Phys.*, **22**, pp.503 – 524 (1995).
3. B. Schaffner, E. Pedroni, A. Lomax , "Dose calculation models for proton treatment planning using a dynamic beam delivery system: an attempt to include density heterogeneity effects in the analytical dose calculation," *Phys Med Biol*., **44**, pp. 27 – 41 (1999).
4. H. Szymanowski and U. Oelfke, "Two-dimensional pencil beam scaling: an improved proton dose algorithm for heterogeneous media," *Phys. Med. Biol*, **47**, pp.3313 – 3330 (2002).
5. H. Jiang and H. Paganetti, "Adaptation of GEANT4 to Monte Carlo dose calculations based on CT data," *Med. Phys.,* **31**, pp 2811 – 2818 (2004).
6. Geant4 Collaboration, "Geant4 – A Simulation Toolkit", *Nuclear Instruments and Methods*, **A506**, pp. 250 – 303 (2003).
7. M. Berger, "Proton Monte Carlo transport program PTRAN", NIST Report NISTIR 5113, NIST, Gaithersburg, USA (1993).
8. L. S. Waters, MCNPX User's Manual, Version 2.4.0, LA-CP_02-408, LANL, USA (2002).
9. L. S. Waters, MCNPX User's Manual, Version 2.3.0, LA-UR-02-2607, LANL, USA (2002).
10. J. F. Ziegler, J. P. Biersack and U. Littmark, "The Stopping and Range of Ions in Solids", Pergamon Press, New York, (2003).
11. H. Palmans, "McPTRAN.CAVITY and McPTRAN.RZ, Monte Carlo codes for the simulation of proton beams and calculation of proton detector perturbation factors," *Monte Carlo 2005 Topical meeting*, Chattannooga, USA, 17-21 April 2005 (this conference).
12. D. E. Bonnett, A. Kacperek, M. A. Sheen and T. E. Saxton, "The 62 MeV proton beam for the treatment of ocular melanoma at Clatterbridge", *Br. J. Radiol.*, **66**, pp.907 - 914 (1993).
13. GEANT4 Low Energy Electromagnetic Physics, http://www.ge.infn.it/geant4/lowE/ (2004).
14. ICRU, "Stopping powers and ranges for protons and alpha particles." International Commission on Radiation Units and Measurements Report 49, Bethesda, USA (1993).
15. V. N. Ivanchenko et al., "Geant4 simulation of energy losses of slow hadrons", CERN-99-121, INFN/AE-99/20 (1999).
16. J. F. Janni. "Proton range-energy tables, 1 keV-10 GeV.", *Atomic Data and Nuclear Tables* **27**, pp 2 – 3 (1982).
17. J. F. Ziegler, "The Stopping of Energetic Light Ions in Elemental Matter", *J. Appl. Phys/Rev. Appl. Phys.*, **85**, pp. 1249 – 1272 (1999).

18. P. V. Vavilov, "Ionization losses of high-energy heavy particles.", *Soviet Physics JETP*, **5**, pp 749 (1957)

19. GEANT4 Physics Reference Manual, http://geant4.web.cern.ch/geant4/G4UsersDocuments/Overview/html/index.html (2004).

20. G.. Z. Molière,"Theorie der Streuung schneller geladener Teilchen II Mehrfach- und Vielfachstreuung", *Z. Naturforsch.*, **3a**, pp. 78-97 (1948).

21. S. Goudsmit and J. L. Saunderson, "Multiple scattering of electrons", *Phys. Rev.*, **57**, pp. 24-29 (1940).

22. H. W. Lewis, "Multiple scattering in an infinite medium", *Phys. Rev.*, **78**, pp. 526-529 (1950).

23. H. Palmans, R. Thomas, M. Simon, S. Duane, A. Kacperek, A. DuSautoy and F. Verhaegen, "A small portable graphite calorimeter for dosimetry in low-energy clinical proton beams", *Phys. Med. Biol.*, **49**, pp. 3737 – 3749 (2004).

24. ICRU, "Clinical Proton Dosimetry Part I: Beam Production, Beam Delivery and Measurement of Absorbed Dose" International Commission on Radiation Units and Measurements Report 59, Bethesda, USA (1998).

6 FIGURES

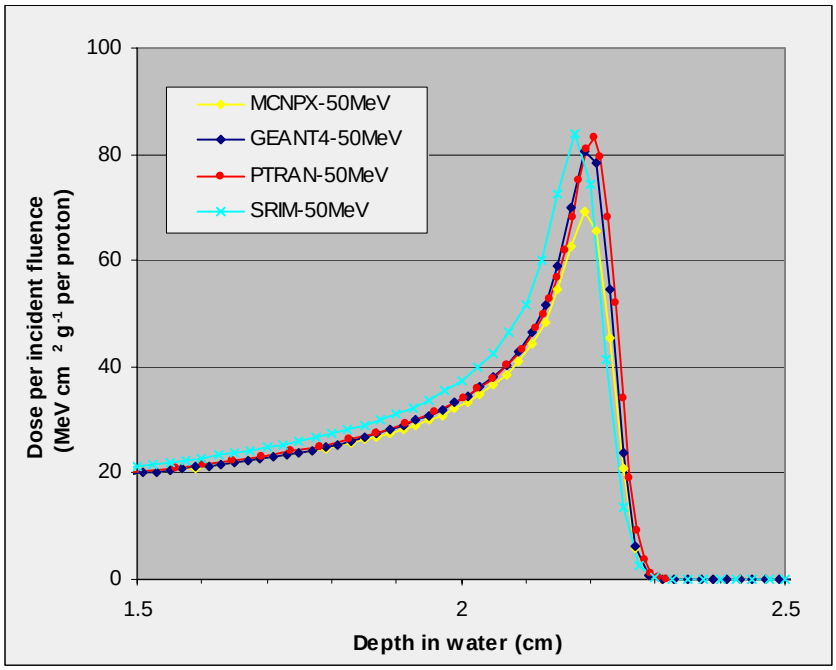

Figure 1: Depth dose curves in water for a 50 MeV monoenergetic pencil beam.

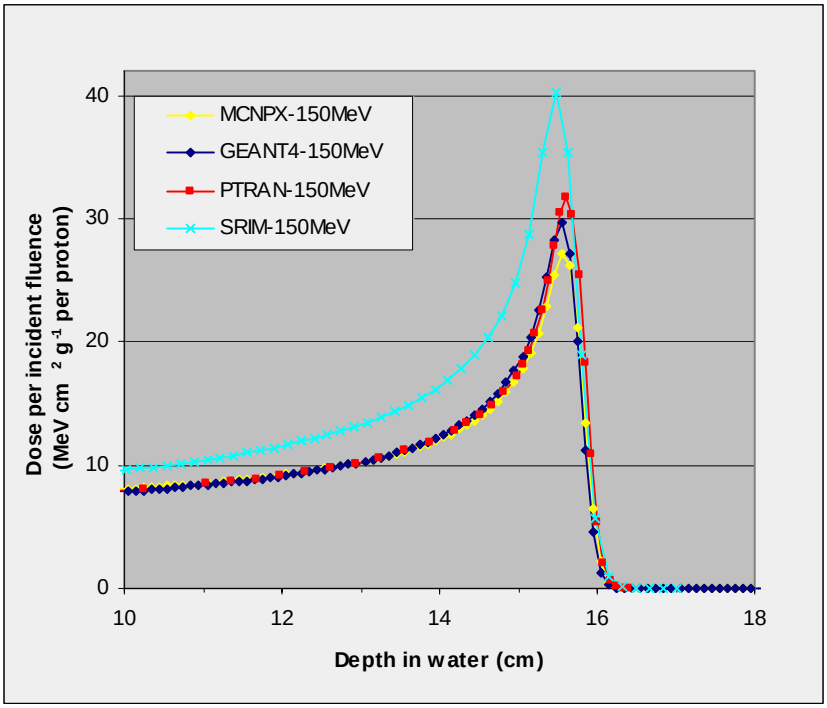

Figure 2: Depth dose curves in water for a 150 MeV monoenergetic pencil beam.

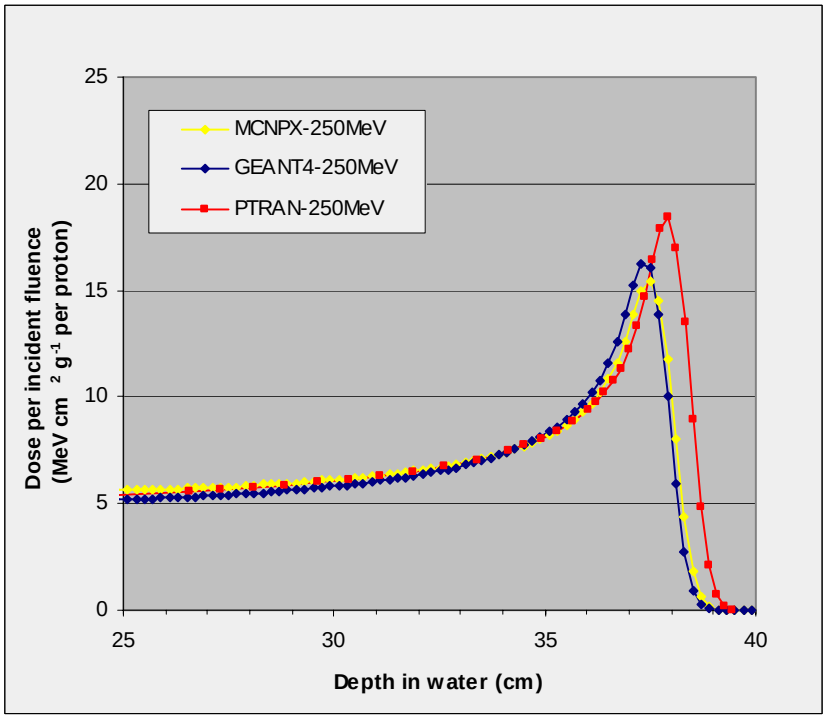

Figure 3 Depth dose curves in water for a 250 MeV monoenergetic pencil beam.

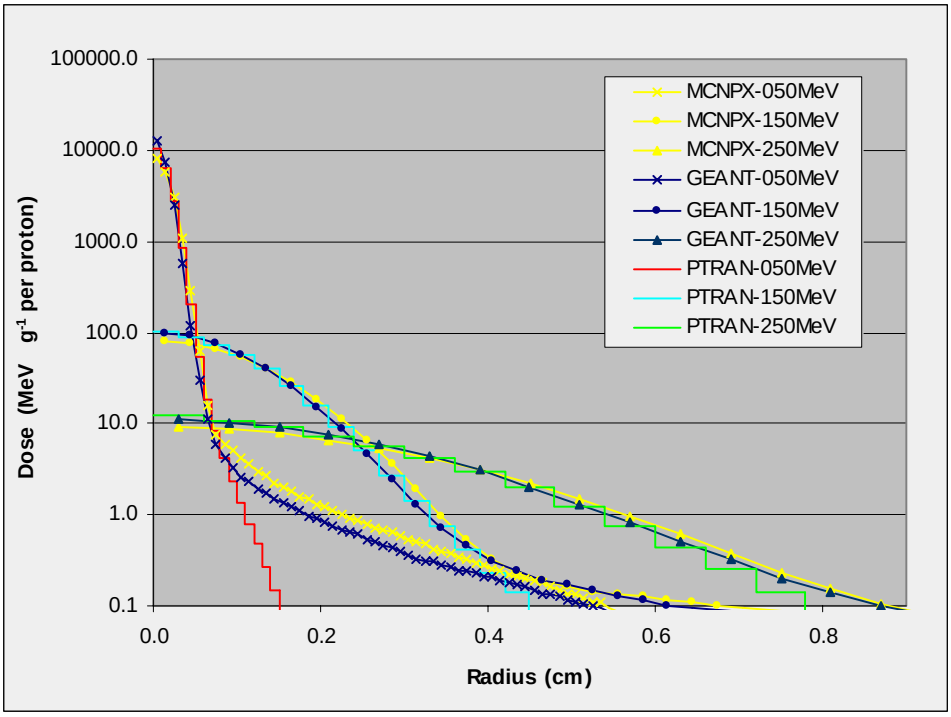

Figure 4: Radial dose distributions in water at $0.5 \times r_0$ for monoenergetic pencil beams.

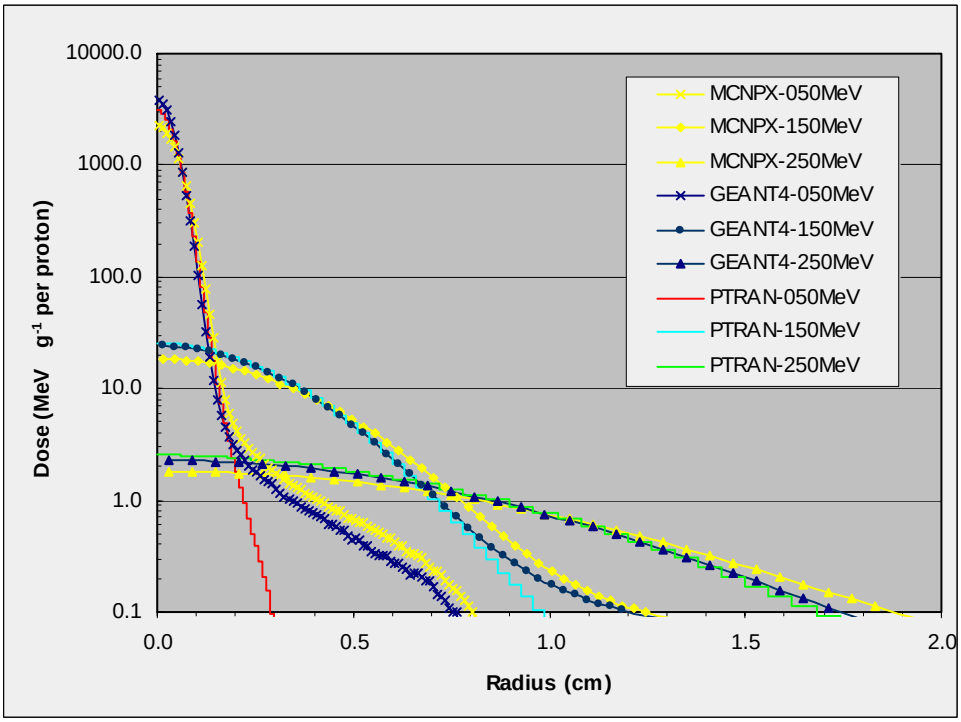

Figure 5: Radial dose distributions in water at $0.9 \times r_0$ for monoenergetic pencil beams.

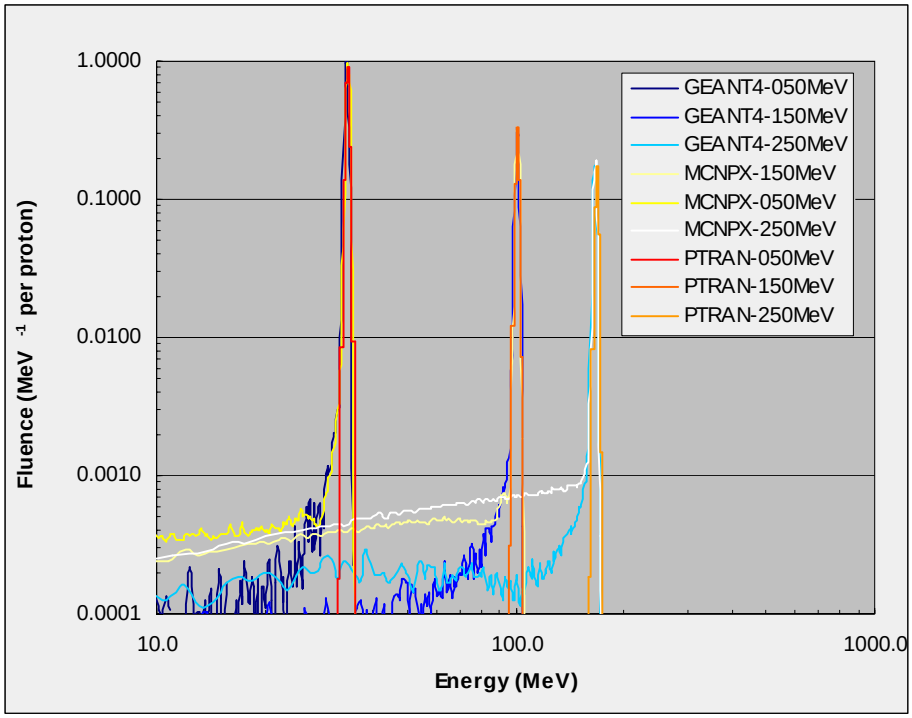

Figure 6: Energy distributions in water at $0.5 \times r_0$ for monoenergetic pencil beams.

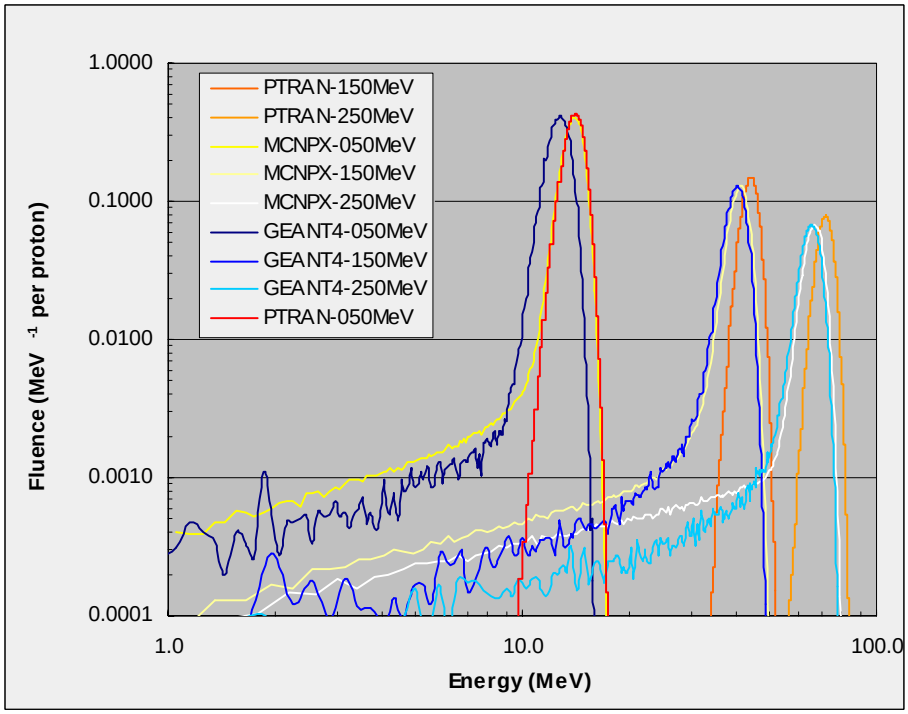

Figure 7: Energy distributions in water at $0.9 \times r_0$ for monoenergetic pencil beams.

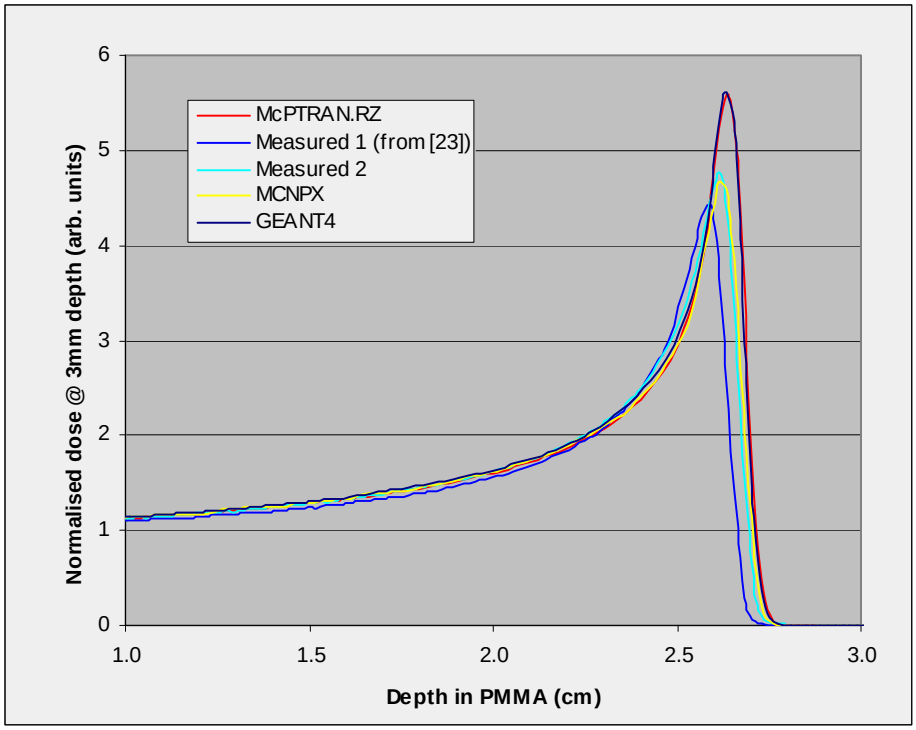

Figure 8: Depth dose in PMMA for the full-energy (no modulator wheel) CCO beam compared with diode measurements. All curves normalised at the entrance dose.

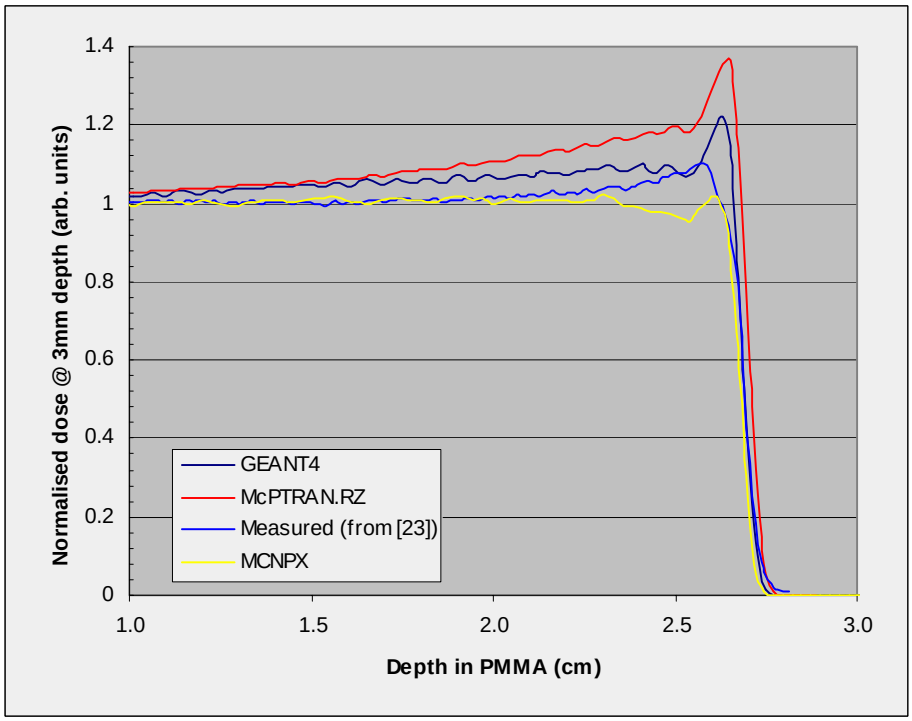

Figure 9: Depth dose in PMMA for the modulated CCO beam compared with diode measurements. All curves normalised at the entrance dose.

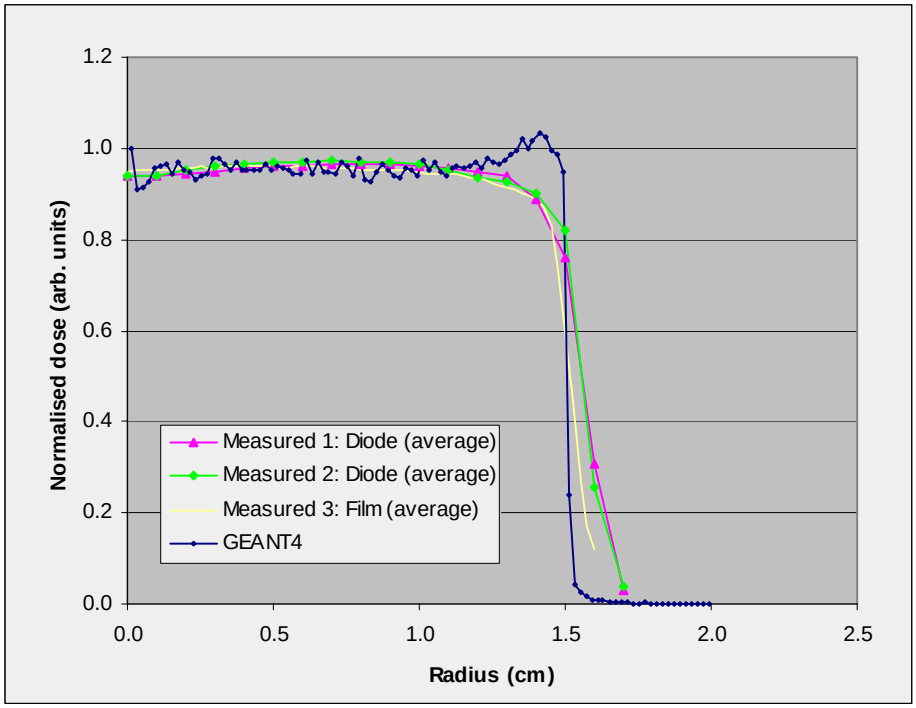

Figure 10: Radial dose distributions at the front face of the phantom for the modulated CCO beam compared with film and diode measurements.

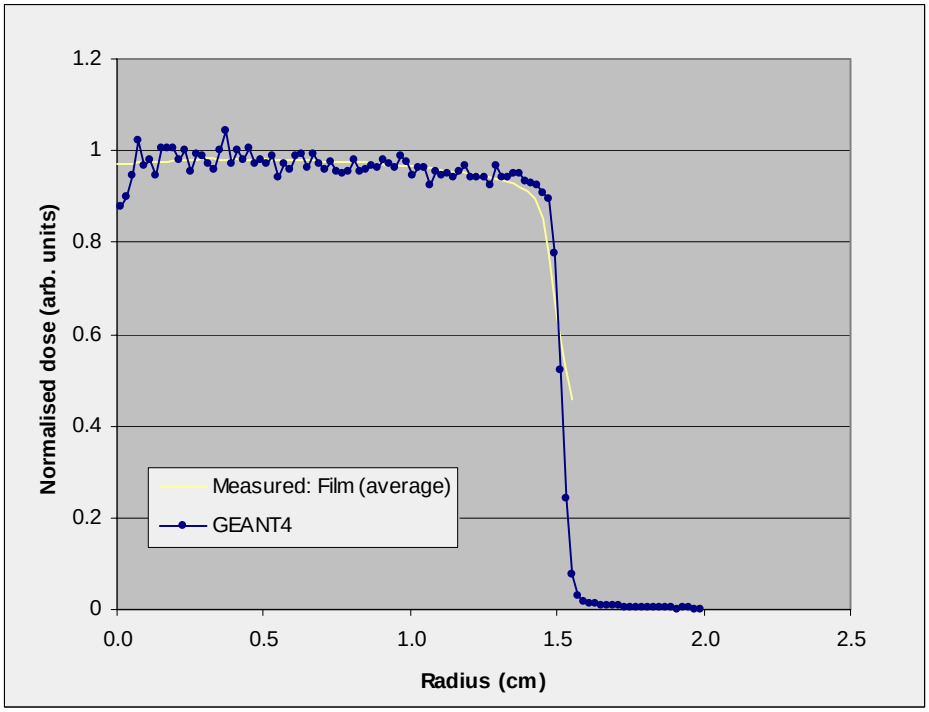

Figure 11: Radial dose distributions at $0.5 \times r_0$ in PMMA for the modulated CCO beam compared with film measurement.